

Hierarchical Ordered Dual-Mesoporous Polypyrrole/Graphene Nanosheets as Bi-Functional Active Materials for High-Performance Planar Integrated System of Micro-Supercapacitor and Gas Sensor

Jieqiong Qin, Jianmei Gao, Xiaoyu Shi, Junyu Chang, Yanfeng Dong, Shuanghao Zheng, Xiao Wang, Liang Feng,* and Zhong-Shuai Wu*

Planar integrated systems of micro-supercapacitors (MSCs) and sensors are of profound importance for 3C electronics, but usually appear poor in compatibility due to the complex connections of device units with multiple mono-functional materials. Herein, 2D hierarchical ordered dual-mesoporous polypyrrole/graphene (DM-PG) nanosheets are developed as bi-functional active materials for a novel prototype planar integrated system of MSC and NH₃ sensor. Owing to effective coupling of conductive graphene and high-sensitive pseudocapacitive polypyrrole, well-defined dual-mesopores of ≈ 7 and ≈ 18 nm, hierarchical mesoporous network, and large surface area of $112 \text{ m}^2 \text{ g}^{-1}$, the resultant DM-PG nanosheets exhibit extraordinary sensing response to NH₃ as low as 200 ppb, exceptional selectivity toward NH₃ that is much higher than other volatile organic compounds, and outstanding capacitance of 376 F g^{-1} at 1 mV s^{-1} for supercapacitors, simultaneously surpassing single-mesoporous and non-mesoporous counterparts. Importantly, the bi-functional DM-PG-based MSC-sensor integrated system represents rapid and stable response exposed to 10–40 ppm of NH₃ after only charging for 100 s, remarkable sensitivity of NH₃ detection that is close to DM-PG-based MSC-free sensor, impressive flexibility with $\approx 82\%$ of initial response value even at 180° , and enhanced overall compatibility, thereby holding great promise for ultrathin, miniaturized, body-attachable, and portable detection of NH₃.

1. Introduction

The rapid progress in portable, wearable, and implantable electronics has intensively spurred micro-electrochemical energy storage devices and their integrated systems.^[1–3] As one competitive miniaturized energy storage unit, micro-supercapacitors (MSCs) constructed on a planar substrate exhibit significant advantages such as separator-free architecture, high power density, fast charge/discharge rate, outstanding cycling stability, and favorable safety.^[4,5] They can be directly integrated with energy harvesters (e.g., solar cell and nanogenerator) and energy consumption units (e.g., digital display and sensor) to realize a self-powered standalone system.^[6–9] In particular, for body-attachable and portable detection of gas pollutants (e.g., NH₃, one of the most common gases in industry, agriculture, and our daily life),^[10–12] the MSC-gas sensor integrated system represents a more and more important core technique of swiftly and reversibly monitoring surrounding gas in real-time to

J. Q. Qin, X. Y. Shi, Dr. S. H. Zheng, X. Wang, Prof. Z.-S. Wu
Dalian National Laboratory for Clean Energy
Dalian Institute of Chemical Physics
Chinese Academy of Sciences
457 Zhongshan Road, Dalian 116023, China
E-mail: wuzs@dicp.ac.cn

J. Q. Qin, J. M. Gao, J. Y. Chang, X. Wang
University of Chinese Academy of Sciences
19 A Yuquan Rd, Shijingshan District, Beijing 100049, China

J. M. Gao, J. Y. Chang, Prof. L. Feng
Department of Instrumentation and Analytical Chemistry
CAS Key Laboratory of Separation Science for Analytical Chemistry
Dalian Institute of Chemical Physics
Chinese Academy of Sciences
457 Zhongshan Road, Dalian 116023, China
E-mail: fengl@dicp.ac.cn

X. Y. Shi
State Key Laboratory of Catalysis
Dalian Institute of Chemical Physics
Chinese Academy of Sciences
457 Zhongshan Road, Dalian 116023, China

X. Y. Shi
Department of Chemical Physics
University of Science and Technology of China
96 Jinzhai Road, Hefei 230026, China

Dr. Y. F. Dong
Department of Chemistry
College of Sciences
Northeastern University
No. 3-11 Wenhua Road, Shenyang 110819, China



The ORCID identification number(s) for the author(s) of this article can be found under <https://doi.org/10.1002/adfm.201909756>.

DOI: 10.1002/adfm.201909756

control industrial processes, reduce environmental pollution, and manage physical health.^[13–15] So far, most integrated systems are assembled with serial devices based on multiple mono-functional materials.^[7,9,16–18] For instance, a MSC-gas sensor integrated system was reported, based on polyaniline-wrapped carbon nanotube MSC as energy storage unit and graphene gas sensor as energy consumption device.^[9] However, the complicated preparation of various mono-functional active materials for single-function energy-related units, and poor compatibility of multiple energy modules involving complex connections, substantially increase the difficulty in the efficient construction of the integrated systems. Recently, Ha's group developed an integrated system of supercapacitor and sensor based on a polydimethylsiloxane coated microporous polypyrrole/graphene foam composite as dual-functional active materials with both high electrochemical and sensing performance, demonstrating the superiority of the supercapacitor-sensor integrated system with dual-functional active materials.^[19] Thus, developing dual-functional active materials with both high energy storage and sensitive sensing performance for planar MSC-gas sensor integrated system is highly desirable.

From the viewpoint of materials, polypyrrole (PPy) possesses tunable electrical conductivity, high electron affinity, reversible redox activity, favorable environmental stability, and excellent biocompatibility, rendering it as a promising high-pseudocapacitive material of supercapacitors and high-sensitive material for NH₃ sensors.^[20–22] Furthermore, graphene has been widely explored for supercapacitors and gas sensors, due to its 2D structure, atomic thickness, large specific surface area, high electrical conductivity, and excellent flexibility.^[23,24] Special emphasis is given to 2D sandwich-like mesoporous nanosheets, chemically assembled by the templating patterning of mesoporous functional species on both surfaces of 2D nanosheets, which can efficiently combine the merits of 2D nanosheets (e.g., graphene) and porous functional materials (e.g., PPy), working together to synergistically generate enhanced electrochemical and gas-sensing performance.^[25–30] Despite the great progress made, the reported 2D sandwich-like mesoporous nanosheets, for example, silica/graphene,^[31] conducting polymers/graphene,^[32,33] carbon/MoS₂,^[34] and Nb₂O₅/graphene,^[35] usually possess only one kind of mesopore, which is not very favorable for fast mass interdiffusion to satisfy the multi-functional devices. In addition, the controllable synthesis of 2D well-defined dual-mesoporous structure keeps a great challenge owing to the difficulty of steering the assembly process in the dual-template system. Therefore, the design and precise synthesis of 2D mesoporous PPy/graphene nanosheets with dual-mesoporous arrays are becoming more reliable and promising, but remain unexplored in one integrated system.

Herein, we first developed hierarchical ordered dual-mesoporous PPy/graphene (DM-PG) nanosheets as bi-functional active materials for a new-concept planar integrated system of MSC and NH₃ sensor. Through a soft and hard dual-template strategy, sandwich-like DM-PG nanosheets, assembled by double PPy layers with well-defined small (≈ 7 nm) and large (≈ 18 nm) mesopore arrays on both sides of graphene, were successfully synthesized. Owing to unique physicochemical feature of PPy/graphene hybrid, 2D nanosheet morphology, uniform thickness of ≈ 80 nm, dual-mesoporous structure, and

high specific surface area of 112 m² g⁻¹, DM-PG nanosheets showed extraordinary sensing response to NH₃ as low as 200 ppb, higher NH₃ response (e.g., 42% to 10 ppm NH₃), and larger specific capacitance (376 F g⁻¹ at 1 mV s⁻¹), compared to single-mesoporous PPy/graphene (SM-PG) nanosheets with mesopores of ≈ 18 nm (19%, 332 F g⁻¹) and non-mesoporous PPy/graphene (NM-PG) nanosheets (10%, 284 F g⁻¹). Further, 2D DM-PG nanosheets severing as bi-functional active materials of MSC and NH₃ sensor realized the facile integration of MSC-sensor system on one planar substrate, presenting high capacitive charge-storage, remarkable sensitivity to NH₃, and favorable flexibility with $\approx 82\%$ of NH₃ response retention even at a bending angle of 180° under room temperature.

2. Results and Discussion

Figure 1 schematically illustrates the precise patterning of DM-PG nanosheets by a soft and hard dual-template method. First, positive-charge graphene oxide (GO) was obtained via the functionalization of polydiallyldimethylammonium chloride, and thus electrostatically adsorbed with negative-charge SiO₂ nanospheres (≈ 7 nm) to assemble 2D SiO₂@GO nanosheets. Then, pyrrole was uniformly polymerized on the surface of SiO₂@GO to form the interior PPy layer on SiO₂@GO nanosheets (PPy/SiO₂@GO). Subsequently, the oxygen-bearing groups on PPy/SiO₂@GO surface interacted with the soft templates of amphiphilic polystyrene-poly(ethylene oxide) (PS₁₅₀-PEO₁₁₄) micelles (PS-PEO) driven by hydrogen bond to uniformly produce the second-layer spherical micelles (PS-PEO@PPy/SiO₂@GO). After polymerization of pyrrole monomers around the building blocks of spherical PS-PEO layer, the exterior PPy array was attained on the surface of PS-PEO@PPy/SiO₂@GO nanosheets (PPy/PS-PEO@PPy/SiO₂@GO). Finally, after the removal of SiO₂ and PS-PEO dual-templates from PPy/PS-PEO@PPy/SiO₂@GO, and hydrothermal reduction of GO interlayer, 2D DM-PG nanosheets were generated.

The morphology and microstructure characterizations of DM-PG nanosheets are displayed in **Figure 2**. Scanning electron microscopy (SEM) images reveal flat and uniform 2D morphology, large lateral size of 1–4 μ m, and highly ordered mesopores (≈ 18 nm) on the top layer of DM-PG nanosheets (**Figure 2a–c**). Transmission electron microscopy (TEM) images confirm the production of hierarchical dual-mesoporous structure, and the coexistence of small mesopores of ≈ 7 nm and large mesopores of ≈ 18 nm (**Figure 2d–f**). Atomic force microscopy (AFM) topography image displays 2D flat structure of DM-PG nanosheets with uniform thickness of ≈ 80 nm (**Figure 2g**), and the homogeneous sphere-like mesoporous structure on the top layer is validated by AFM phase image (**Figure 2h**). N₂ adsorption and desorption isotherm of DM-PG nanosheets suggests the typical IV-type curve with the hysteresis loop of H2-type (**Figure 2i**), presenting high specific surface area of 112 m² g⁻¹ and large pore volume of 0.30 cm³ g⁻¹. Notably, the dual-mesoporous feature is further confirmed by the pore size distribution curve, showing two obvious peaks of ≈ 7 nm and ≈ 18 nm (inset in **Figure 2i**), consistent with TEM observation. Furthermore, FT-IR spectrum of DM-PG nanosheets exhibits the characteristic peaks of C=C bonds at 1550 and 1470 cm⁻¹,

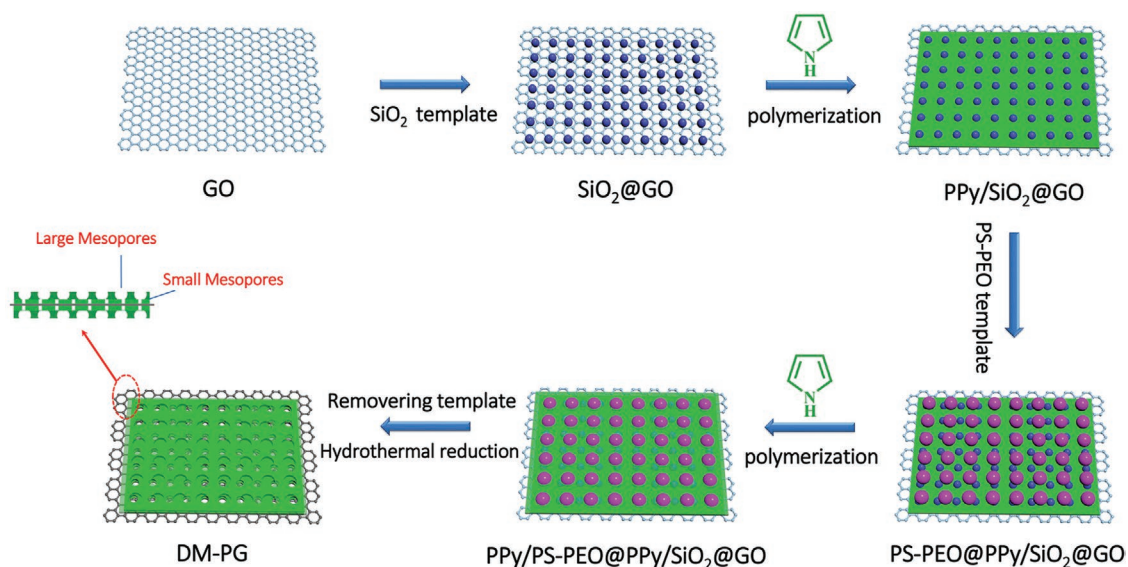


Figure 1. Schematic illustration of the precise synthesis of 2D DM-PG nanosheets.

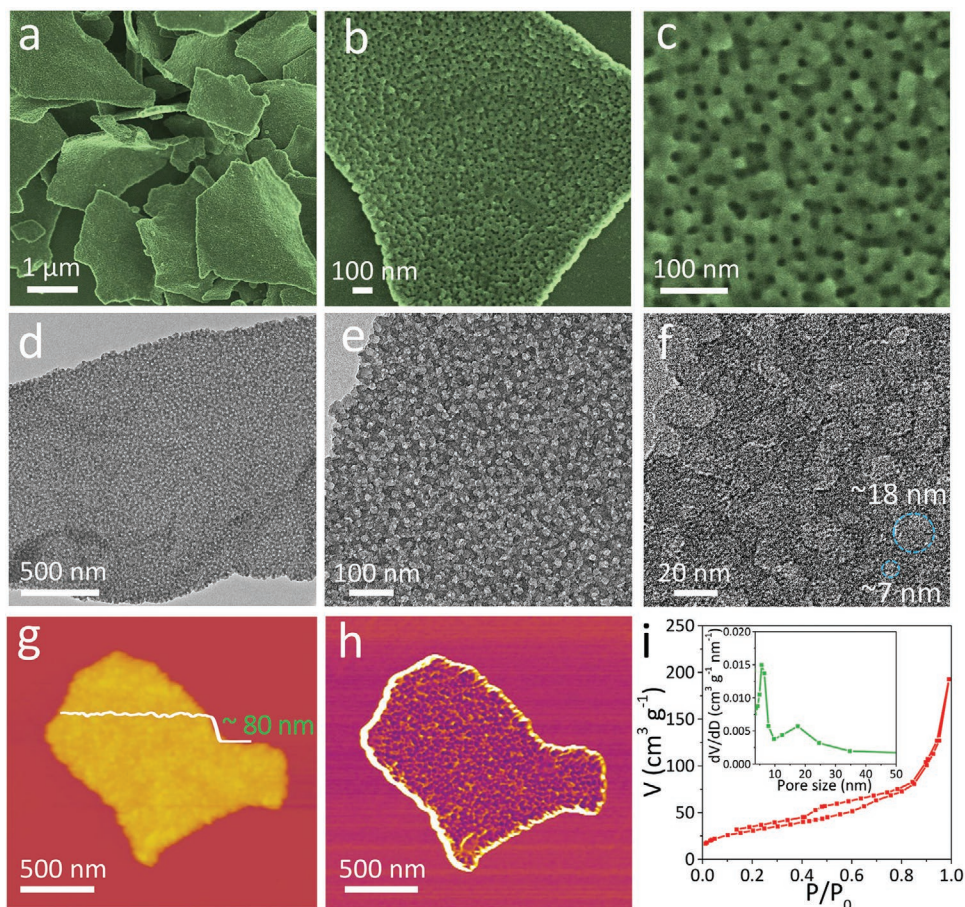


Figure 2. Morphology and microstructure of 2D DM-PG nanosheets. a–c) SEM images of DM-PG nanosheets. d,e) TEM and f) HRTEM images of DM-PG nanosheets. g) AFM topography image and corresponding height profile, and h) AFM phase image of DM-PG nanosheets. i) N₂ adsorption and desorption isotherm, and pore size distribution (inset) of DM-PG nanosheets.

N–H groups at 1645 and 1375 cm^{-1} , C–N bonds at 1279 cm^{-1} , and C–H groups at 1035 cm^{-1} assigning to PPy and reduced graphene oxide (rGO),^[32,33,36] indicative of the successful hybridization of rGO and PPy in DM-PG nanosheets (Figure S1, Supporting Information). Raman spectrum of DM-PG nanosheets displays the D and G peaks of graphene at 1350 and 1590 cm^{-1} , partially overlapped with the peaks of PPy at 1330 and 1570 cm^{-1} (Figure S2, Supporting Information).^[32,33] Moreover, the lower intensity ratio of I_D/I_G (1.04) than that ($I_D/I_G = 1.16$) before reduction (Figure S3, Supporting Information) suggests the efficient reduction of GO.^[37–39] It is noteworthy that the selection of appropriate mesopore templates is crucial for the generation of dual-mesopores. When using either two soft templates or two hard templates, the as-synthesized 2D hybrid nanosheets only show heterogeneous mesoporous morphology (Figures S4 and S5, Supporting Information).

Owing to the effective coupling of high-sensitive, pseudocapacitive PPy and electrically conductive graphene, hierarchical ordered dual-mesopores, and large specific surface area, the as-obtained DM-PG nanosheets are expected to serve as bi-functional active materials for gas sensor and supercapacitors. To demonstrate the importance of hierarchical order dual-mesopores in DM-PG nanosheets, we further synthesized the counterparts of SM-PG and NM-PG nanosheets (Figures S6–S8, Supporting Information), and compared their gas sensing and electrochemical performance. First, the NH_3 sensing properties of DM-PG, SM-PG, and NM-PG nanosheets were examined by drop-coating their dispersion (20 μL , 1 mg mL^{-1} in ethanol) on ceramic tube with Au electrodes (Figure S9, Supporting Information). The real-time dynamic changes in resistance toward NH_3 of 200 ppb and 40 ppm were examined for DM-PG, SM-PG, and NM-PG at room temperature (Figure 3a; Figure S10, Supporting Information). The whole sensing process delivers a quick positive response in 5 min and recovery within 10 min, resulting from the classical p-type semiconductor characteristic of PPy in reducing gas.^[15,21] Moreover, these three sensors reveal concentration-dependent behavior and reversible response upon continuous exposure/release cycles. Notably, DM-PG based sensor presents much higher response value (e.g., 42% at 10 ppm NH_3), which is better than those of SM-PG (19%) and NM-PG (10%) (Figure 3b), and outperforms most reported PPy based NH_3 sensors, such as PPy nanowires (5% response at 10 ppm NH_3),^[40] PPy/rGO (7% response at 25 ppm NH_3),^[41] PPy nanowires/nanoparticles (4% response at 50 ppm NH_3),^[42] PPy-rGO/polyaniline (PANI) (15% response at 10 ppm NH_3),^[43] PPy/rGO (6% response at 1 ppm NH_3),^[44] and PPy/graphene (10% response at 5 ppm NH_3)^[45] (Table S1, Supporting Information). Meanwhile, DM-PG nanosheets reveal favorable response and

recovery rates compared with other reported PPy based NH_3 sensors, and the recovery time can be shortened significantly by heating (Figure S11, Supporting Information). These results confirm the great advantage of DM-PG nanosheets for gas sensors, owing to hierarchical ordered dual-mesoporous structure for boosting carrier transfer.^[46–48] The selectivity of DM-PG nanosheets were further examined upon NH_3 of 40 ppm and other volatile organic compounds and water of 500 ppm, including ethanol, methanol, acetone, acetonitrile, chlorobenzene, ethyl acetate, toluene, and tetrachloromethane (Figure 3c). Remarkably, the response value of DM-PG based sensor is as high as $\approx 56\%$, at least 29 times higher than those of other interfering gases even with higher concentrations, indicative of exceptional selectivity of DM-PG nanosheets toward NH_3 . Also, our DM-PG based sensor presents negligible response toward the mixture of these interfering gases compared to that ($\approx 57\%$ response) once injecting 40 ppm NH_3 , further demonstrative of outstanding anti-interference property of DM-PG nanosheets (Figure S12, Supporting Information). Furthermore, the reproducibility of DM-PG based sensor was evaluated during periodic exposures to 2 ppm NH_3 every 24 h for 7 cycles and continuous cycling measurements of 5 cycles (Figure 3d; Figure S13, Supporting Information). Notably, slight fluctuations of DM-PG based NH_3 sensor are observed, demonstrative of outstanding

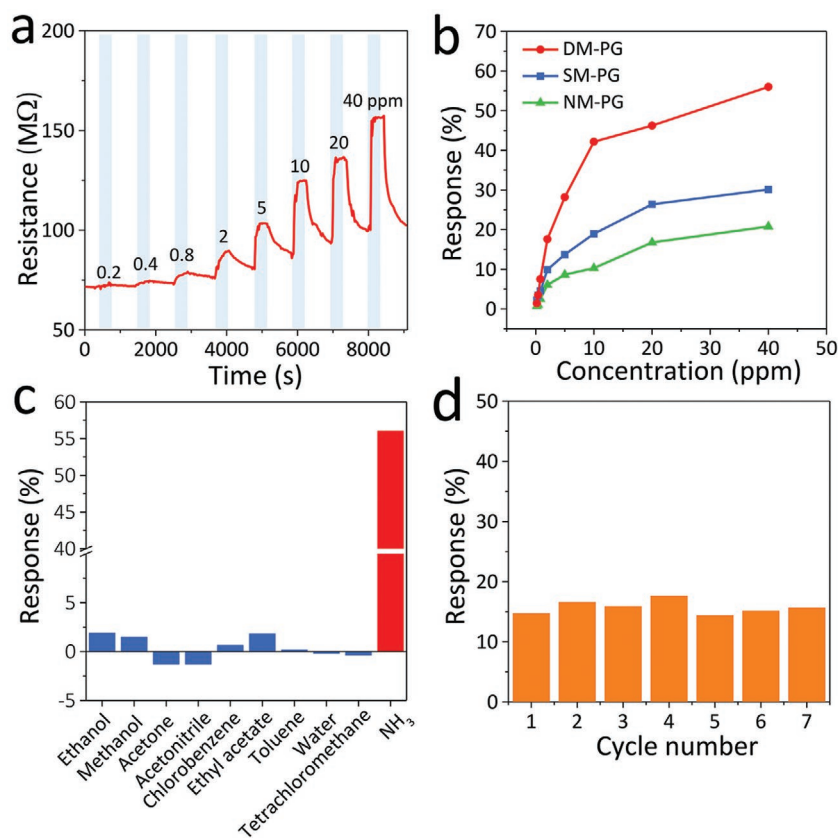


Figure 3. Gas sensing performance of 2D DM-PG, SM-PG, and NM-PG nanosheets. a) Real-time dynamic response curves of DM-PG with NH_3 concentration from 200 ppb to 40 ppm at room temperature. b) Response of DM-PG, SM-PG, and NM-PG nanosheets as a function of NH_3 concentration. c) Selectivity of DM-PG to 40 ppm NH_3 and 500 ppm other gas. d) Cycling stability of DM-PG based sensor with 2 ppm NH_3 tested every 24 h for 7 cycles.

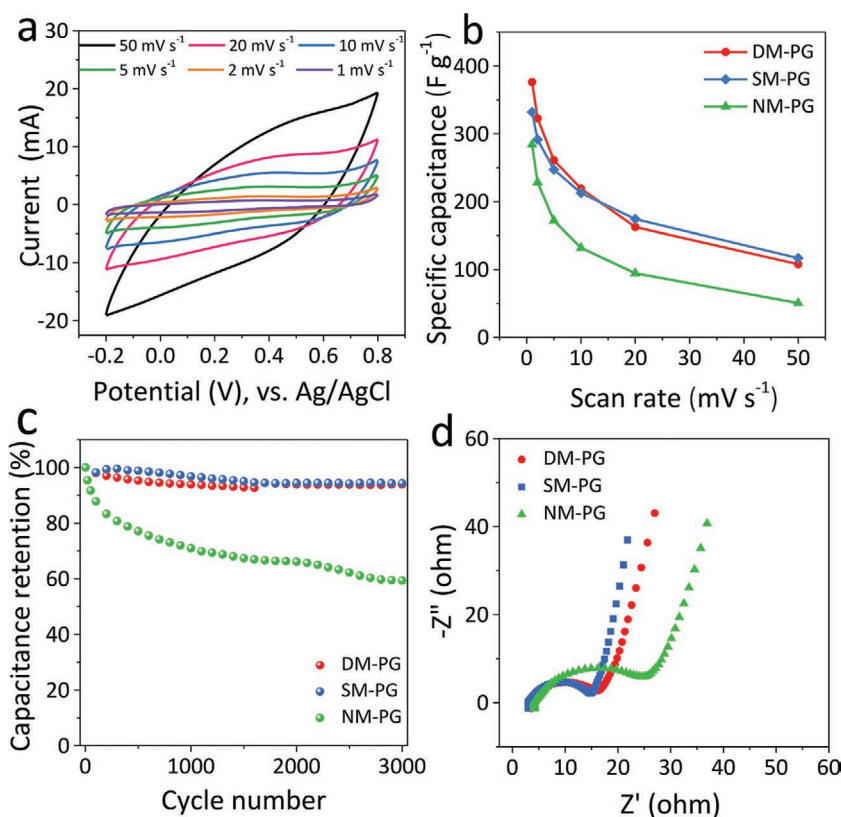


Figure 4. Electrochemical performance of 2D DM-PG, SM-PG, and NM-PG nanosheets. a) CV curves of DM-PG obtained at scan rates from 1 to 50 mV s⁻¹, tested in 1 M H₂SO₄. b) Specific capacitance as a function of scan rate. c) cycling stability for 3000 cycles, and d) EIS plots of DM-PG, SM-PG, and NM-PG nanosheets.

reproducibility. These results manifest that DM-PG nanosheets hold great potential as sensing material to sensitively, selectively, and steadily detect NH₃ at room temperature. The sensing mechanism can be explained by the p-type semiconductor behavior of PPy in sensing process, in which the reducing NH₃ gas as electron donor can neutralize the holes in the PPy along with electrons transfer from NH₃ molecule to the π backbone of PPy, resulting in the reduction of charge carrier concentration in DM-PG and the increase of the sensor resistance.^[12,21,44,49]

Further, we carried out the electrochemical performance of DM-PG, SM-PG, and NM-PG nanosheets by cyclic voltammetry (CV) curves, galvanostatic charge/discharge (GCD) profiles and electrochemical impedance spectroscopy (EIS) in a three-electrode system at 1 M H₂SO₄ electrolyte. The CV curves measured at scan rates from 1 to 50 mV s⁻¹ of DM-PG show obviously surface-dominated pseudocapacitive behavior derived from PPy (Figure 4a). Also, DM-PG nanosheets present bigger integration area in CV curves (at 10 mV s⁻¹), and longer discharge time in GCD profiles (at 1 A g⁻¹) in comparison with SM-PG and NM-PG nanosheets (Figure S14, Supporting Information). As a result, DM-PG yields higher capacitance of 376 F g⁻¹ at 1 mV s⁻¹ than SM-PG (332 F g⁻¹) and NM-PG (284 F g⁻¹) (Figure 4b), demonstrative of the superiority of dual-mesoporous arrays. Moreover, DM-PG nanosheets deliver favorable rate capability with 108 F g⁻¹ at high scan rate of 50 mV s⁻¹, which is comparable to SM-PG (117 F g⁻¹) and

higher than NM-PG (51 F g⁻¹). Both DM-PG and SM-PG nanosheets maintain $\approx 94\%$ of initial capacitance in comparison with NM-PG (60%) after 3000 cycles (Figure 4c), suggestive of the significance of mesoporous structure. EIS plots represents lower equivalent series resistance of 16 Ω for DM-PG and 15 Ω for SM-PG than that of NM-PG (27 Ω), and larger slope in the low frequency range for DM-PG and SM-PG, indicative of enhanced ion diffusion transport from mesoporous nanosheets (Figure 4d).

To evaluate the potential of DM-PG nanosheets for practical energy storage, we further employ 2D DM-PG as interdigital microelectrodes to construct all-solid-state planar DM-PG MSC using a mask-assisted deposition technique,^[50-53] with the assistance of electrochemically exfoliated graphene (EG) as metal-free current collector,^[54-56] carbon nanotube (CNT) as conductive additive, and polyvinyl alcohol (PVA)/H₂SO₄ gel as electrolyte (Figure 5a; Figure S15, Supporting Information). It is noted that the addition of CNT into microelectrodes can guarantee large-area continuity, robust mechanical flexibility, and high performance (Figures S16 and S17, Supporting Information). Cross-section SEM image discloses compact layered structure of DM-PG microelectrodes with a thickness of 3.4 μm (Figure 5b), while top-view SEM image reveals outstanding structural integrity and flat surface morphology of

microelectrode (Figure 5c). Significantly, DM-PG MSC delivers impressive pseudocapacitive behavior, and stepwise increasing current with increasing scan rates, as seen from CV curves (Figure 5d). The maximum areal capacitance of 38 mF cm⁻² as well as volumetric capacitance of 110 F cm⁻³ are obtained at 1 mV s⁻¹ for DM-PG MSC (Figure 5e), both of which are much higher than those graphene and conducting polymer based MSCs, for example, laser-reduced rGO (2.0 mF cm⁻² and 12.4 F cm⁻³),^[57] plasma-reduced rGO (0.32 mF cm⁻² and 71.6 F cm⁻³),^[58] and PANI/rGO (13 mF cm⁻² and 66.2 F cm⁻³)^[59] (Table S2, Supporting Information). Further, DM-PG MSC displays favorable cycling stability with capacitance retention of 82% after 4500 cycles (Figure S18, Supporting Information). Ragone plot of DM-PG MSC is given in Figure 5f. Remarkably, our DM-PG MSC provides a volumetric energy density of 2.5 mWh cm⁻³, which is higher than those of commercially available supercapacitors (<1.0 mWh cm⁻³) and Al electrolytic capacitors (<2.0 $\mu\text{Wh cm}^{-3}$),^[56,60,61] and exceeds many recently reported conducting polymer based MSCs, such as PANI nanowires (0.78 mWh cm⁻³),^[62] PANI/rGO (1.51 mWh cm⁻³),^[59] and parallel cylindrical mesoporous PPy/rGO (2.3 mWh cm⁻³)^[33] (Table S2, Supporting Information). Meanwhile, DM-PG MSC delivers an impressive volumetric power density of 397 mW cm⁻³ at energy density of 0.9 mWh cm⁻³. It is noted that the volumetric power density can be improved by increasing the electrical conductivity of EG current collector

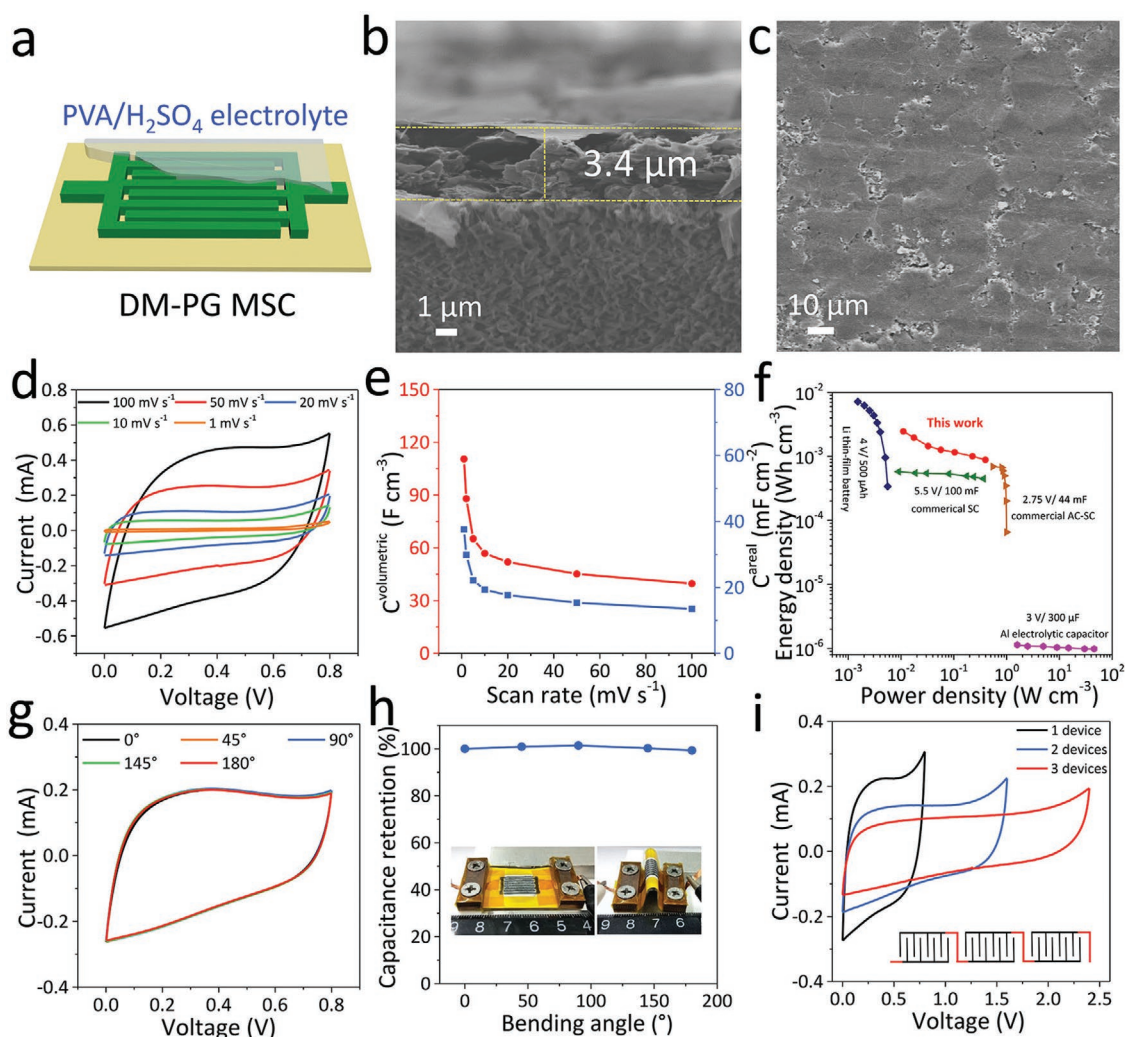


Figure 5. Electrochemical performance of DM-PG MSC. a) Schematic of DM-PG MSC. b) Cross section and c) top-view SEM images of DM-PG microelectrode film. d) CV curves of DM-PG MSC tested at different scan rates of 1–100 mV s^{-1} . e) Volumetric and areal capacitances as a function of scan rate. f) Ragone plot of DM-PG MSC and commercially available energy storage devices. g) CV curves of DM-PG MSC collected at 50 mV s^{-1} under different bending angles. h) Capacitance retention as a function of bending angle for DM-PG MSC (Insets: optical photographs of the MSC taken at bending angles of 0° and 180°). i) CV curves tested at 50 mV s^{-1} for serially-connected DM-PG MSCs.

(Figure S19, Supporting Information). To verify the flexibility of DM-PG MSC, we accessed their electrochemical performance under varying bending states. As shown in Figure 5g,h, DM-PG MSC displays almost overlapped CV curves with varying bending angles, and $\approx 99\%$ capacitance retention even at a high bending angle of 180° , indicative of outstanding flexibility and structural stability. Furthermore, serially-connected DM-PG MSCs reveal the progressive voltage extension from 0.8 V for single cell to 2.4 V for three cells, and integrated DM-PG MSCs in parallel display the stepwise linear increase of capacitance (Figure 5i; Figures S20 and S21, Supporting Information), demonstrative of extraordinary performance uniformity.

Considering the bi-functional properties of 2D DM-PG nanosheets for high-performance sensor and MSC individually, we constructed a prototype planar MSC-sensor integrated system based on this hierarchical ordered dual-mesoporous nanosheet for MSC as power source and gas sensor for NH_3

detection. To enhance the compatibility of MSC-sensor modules and simplify the integration process, a mask-assisted deposition strategy was used for simultaneous fabrication of highly integrated planar MSC-sensor system (Figure 6a). It is noted that high conducting EG nanosheets are employed as interdigital current collector and metal-free interconnection for MSC and sensor. As shown in Figure 6b,c, the microelectrodes of MSC-sensor integrated system exhibit outstanding continuity and excellent mechanical flexibility. After drop-casting PVA/ H_2SO_4 electrolyte on the microelectrodes of MSC and DM-PG active materials on sensor region, the planar MSC-sensor integrated system is obtained, in which DM-PG MSC with relatively stable output voltage (Figure S22, Supporting Information) can be applied to power DM-PG based sensor. The sensing performance of this MSC-driven sensor upon NH_3 was recorded by the variation of partial voltage (Inset in Figure 6c). It can be seen that, after charging for 100 s, the

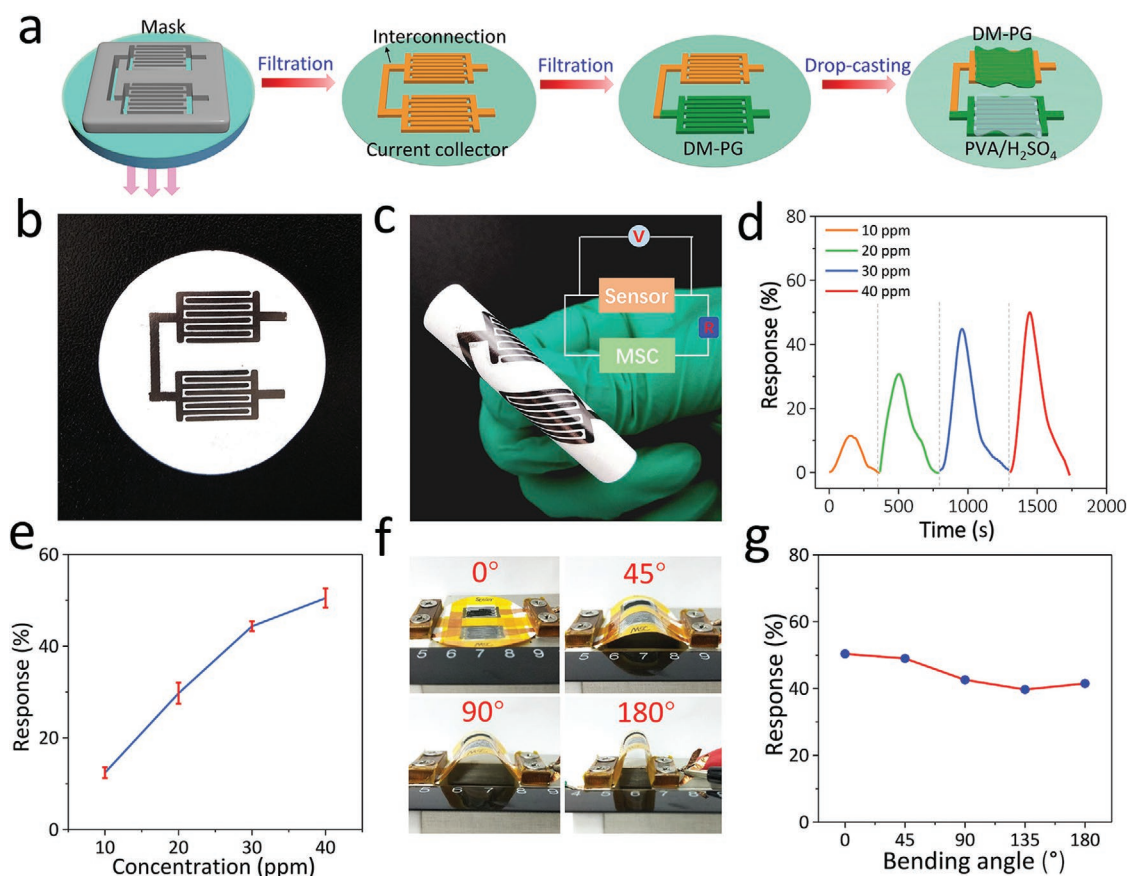


Figure 6. Characterizations and performance of the planar MSC-sensor integrated system. a) Schematic diagram of the fabrication of planar MSC-sensor integrated system. Photographs of microelectrodes of planar MSC-sensor integrated system at b) flat and c) bending states. Inset in (c) is the equivalent circuit of planar MSC-sensor integrated system. d) Response curves of MSC-driven sensor upon exposure to NH_3 of 10–40 ppm (intermittent testing). e) Response of MSC-driven sensor as a function of NH_3 concentration from 10 to 40 ppm. f) Optical images of planar MSC-sensor integrated system taken at various bending angles. g) Response of MSC-driven sensor as a function of bending angle to 40 ppm NH_3 .

MSC-driven sensor reveals rapid and stable response exposed to 10–40 ppm of NH_3 at room temperature (Figure 6d). The response significantly improves with increasing NH_3 concentration and presents small standard deviation of no more than 2.5% at same NH_3 concentration (Figure 6d,e). At 40 ppm NH_3 , the response value of our MSC-driven sensor is 50%, which is very close to that of the traditional DM-PG based sensor (56%) without MSC, demonstrative of the feasibility and uniqueness of our integrated system. Prominently, our MSC-driven sensor also can realize continuous, long-time, and steady operation under periodic exposure to 40 ppm NH_3 or 10–40 ppm NH_3 once DM-PG MSC is fully charged in 100 s, suggestive of outstanding sensing reliability (Figures S23 and S24, Supporting Information). Moreover, the planar MSC-sensor integrated system can steadily work at varying bending angles and remain $\approx 82\%$ of initial response value even at a high bending angle of 180° , indicative of exceptional flexibility and stability of this planar integrated system (Figure 6f,g).

The superior performance of planar MSC-sensor integrated system is attributed to the elaborated design of hierarchical ordered dual-mesoporous DM-PG nanosheets as bi-functional active materials with enhanced compatibility for MSC and sensor simultaneously. First, DM-PG nanosheets feature

synergistic coupling of high-sensitive, pseudocapacitive PPy and conductive graphene, endowing them with the combined merits of individual materials while eliminating their related drawbacks for high-performance gas sensors and supercapacitors. Second, 2D hierarchical ordered dual-mesoporous structure of DM-PG nanosheets offers abundant porous networks and large specific surface area, significantly promoting fast gas adsorption/desorption for sensor, and rapid ion diffusion and fast electron transfer for supercapacitor. Third, bi-functional DM-PG nanosheets as active materials of MSC and NH_3 sensor can greatly simplify the complicated preparation of multiple mono-functional materials for single energy-related unit, and enhance the overall compatibility of MSC-sensor integrated system. Fourth, the MSC-sensor integrated microsystem with planar configuration and graphene current collectors, can offer high conductive network and more accessible active sites for high energy storage and rapid NH_3 response. Last but not the least, thin thickness and excellent flexibility of 2D DM-PG nanosheets afford rapid ion transport along the plane and 2D nanochannels between nanosheets for maximizing charge storage, and desirable suppleness of the whole device, significantly improving the performance of the integrated system in a planar geometry.^[23,63–65]

3. Conclusion

In summary, we have developed one bi-functional material of 2D DM-PG nanosheets with hierarchical ordered dual-mesopores for the planar MSC-sensor integrated system on one single substrate, in which MSC serves as microscale power source and sensor for sensitively detecting NH₃ gas. Compared with SM-PG and NM-PG nanosheets, DM-PG nanosheets deliver remarkably enhanced NH₃ response for gas sensor and improved capacitance for supercapacitors, verifying the superiority of hierarchical ordered dual-mesopores. Further, using bi-functional DM-PG nanosheets as active materials, all-solid-state MSC and planar NH₃ sensor realize simplified fabrication and seamless integration. The MSC-sensor integrated system unveils high capacitive performance, exceptional flexibility, and high NH₃ sensitivity at room temperature. Therefore, this strategy of developing 2D hierarchical ordered dual-mesoporous nanosheets for planar MSC-sensor integrated system will offer many opportunities to create the ultrathin, miniaturized, flexible, self-powered electronics for personalized healthcare, environmental protection, and biomedical monitoring.

Supporting Information

Supporting Information is available from the Wiley Online Library or from the author.

Acknowledgements

The authors acknowledge the financial support from National Key R&D Program of China (2016YFA0200200), National Natural Science Foundation of China (51702078, 51572259, and 51872283), Natural Science Foundation of Liaoning Province, Joint Research Fund Liaoning-Shenyang National Laboratory for Materials Science (20180510038), Liaoning Revitalization Talents Program (XLYC1807153), DICP (ZZBS201708, and ZZBS201802), DICP&QIBEBT (UN201702), and Dalian National Laboratory For Clean Energy (DNL), CAS, DNL Cooperation Fund, CAS (DNL180310, DNL180308, DNL201912, and DNL201915).

Conflict of Interest

The authors declare no conflict of interest.

Keywords

dual-mesopores, micro-supercapacitors, planar integrated systems, polypyrrole/graphene nanosheets sensor

Received: November 21, 2019

Revised: January 12, 2020

Published online: February 24, 2020

- [1] J. A. Rogers, T. Someya, Y. G. Huang, *Science* **2010**, 327, 1603.
[2] A. Sumboja, J. Liu, W. G. Zheng, Y. Zong, H. Zhang, Z. Liu, *Chem. Soc. Rev.* **2018**, 47, 5919.

- [3] S. Zheng, X. Shi, P. Das, Z.-S. Wu, X. Bao, *Adv. Mater.* **2019**, 31, 1900583.
[4] Z.-S. Wu, X. Feng, H.-M. Cheng, *Natl. Sci. Rev.* **2014**, 1, 277.
[5] J. Wang, F. Li, F. Zhu, O. G. Schmidt, *Small Methods* **2019**, 3, 1800367.
[6] J. Ye, H. Tan, S. Wu, K. Ni, F. Pan, J. Liu, Z. Tao, Y. Qu, H. Ji, P. Simon, Y. Zhu, *Adv. Mater.* **2018**, 30, 1801384.
[7] J. Yun, C. Song, H. Lee, H. Park, Y. R. Jeong, J. W. Kim, S. W. Jin, S. Y. Oh, L. Sun, G. Zi, J. S. Ha, *Nano Energy* **2018**, 49, 644.
[8] J. Yun, Y. Lim, H. Lee, G. Lee, H. Park, S. Y. Hong, S. W. Jin, Y. H. Lee, S.-S. Lee, J. S. Ha, *Adv. Funct. Mater.* **2017**, 27, 1700135.
[9] J. Yun, Y. Lim, G. N. Jang, D. Kim, S.-J. Lee, H. Park, S. Y. Hong, G. Lee, G. Zi, J. S. Ha, *Nano Energy* **2016**, 19, 401.
[10] W. Luo, T. Zhao, Y. Li, J. Wei, P. Xu, X. Li, Y. Wang, W. Zhang, A. A. Elzatahry, A. Alghamdi, Y. Deng, L. Wang, W. Jiang, Y. Liu, B. Kong, D. Zhao, *J. Am. Chem. Soc.* **2016**, 138, 12586.
[11] Y. Wang, J. Liu, X. Cui, Y. Gao, J. Ma, Y. Sun, P. Sun, F. Liu, X. Liang, T. Zhang, G. Lu, *Sens. Actuators, B* **2017**, 238, 473.
[12] T. Yoon, J. Jun, D. Y. Kim, S. Pourasad, T. J. Shin, S. U. Yu, W. Na, J. Jang, K. S. Kim, *J. Mater. Chem. A* **2018**, 6, 2257.
[13] H. Nazemi, A. Joseph, J. Park, A. Emadi, *Sensors* **2019**, 19, 1285.
[14] K. Arshak, *Sens. Rev.* **2004**, 24, 181.
[15] T. Wagner, S. Haffer, C. Weinberger, D. Klaus, M. Tiemann, *Chem. Soc. Rev.* **2013**, 42, 4036.
[16] J. Zhao, L. Li, Y. Zhang, C. Li, Q. Zhang, J. Peng, X. Zhao, Q. Li, X. Wang, J. Xie, J. Sun, B. He, C. Lu, W. Lu, T. Zhang, Y. Yao, *Energy Storage Mater.* **2018**, 15, 315.
[17] J. Zhao, Y. Zhang, Y. Huang, J. Xie, X. Zhao, C. Li, J. Qu, Q. Zhang, J. Sun, B. He, Q. Li, C. Lu, X. Xu, W. Lu, L. Li, Y. Yao, *Adv. Sci.* **2018**, 5, 1801114.
[18] Y. Lin, J. Chen, M. M. Tavakoli, Y. Gao, Y. Zhu, D. Zhang, M. Kam, Z. He, Z. Fan, *Adv. Mater.* **2019**, 31, 1804285.
[19] H. Park, J. W. Kim, S. Y. Hong, G. Lee, D. S. Kim, J. H. Oh, S. W. Jin, Y. R. Jeong, S. Y. Oh, J. Y. Yun, J. S. Ha, *Adv. Funct. Mater.* **2018**, 28, 1707013.
[20] Y. Shi, L. Peng, Y. Ding, Y. Zhao, G. Yu, *Chem. Soc. Rev.* **2015**, 44, 6684.
[21] H. Bai, G. Shi, *Sensors* **2007**, 7, 267.
[22] M. Xue, F. Li, D. Chen, Z. Yang, X. Wang, J. Ji, *Adv. Mater.* **2016**, 28, 8265.
[23] Y. Zhu, S. Murali, W. Cai, X. Li, J. W. Suk, J. R. Potts, R. S. Ruoff, *Adv. Mater.* **2010**, 22, 3906.
[24] W. Yuan, G. Shi, *J. Mater. Chem. A* **2013**, 1, 10078.
[25] Y. Xu, Z. Lin, X. Zhong, X. Huang, N. O. Weiss, Y. Huang, X. Duan, *Nat. Commun.* **2014**, 5, 4554.
[26] K. Lan, Y. Liu, W. Zhang, Y. Liu, A. Elzatahry, R. Wang, Y. Xia, D. Al-Dhayan, N. Zheng, D. Zhao, *J. Am. Chem. Soc.* **2018**, 140, 4135.
[27] S. Liu, F. Wang, R. Dong, T. Zhang, J. Zhang, X. Zhuang, Y. Mai, X. Feng, *Adv. Mater.* **2016**, 28, 8365.
[28] Y. Fang, Y. Lv, R. Che, H. Wu, X. Zhang, D. Gu, G. Zheng, D. Zhao, *J. Am. Chem. Soc.* **2013**, 135, 1524.
[29] S. B. Yang, X. L. Feng, K. Müllen, *Adv. Mater.* **2011**, 23, 3575.
[30] W. Wu, C. Zhang, S. Yang, *New Carbon Mater.* **2017**, 32, 1.
[31] S. B. Yang, X. L. Feng, L. Wang, K. Tang, J. Maier, K. Müllen, *Angew. Chem., Int. Ed.* **2010**, 49, 4795.
[32] S. Liu, P. Gordiichuk, Z.-S. Wu, Z. Liu, W. Wei, M. Wagner, N. Mohamed-Noriega, D. Wu, Y. Mai, A. Herrmann, K. Müllen, X. Feng, *Nat. Commun.* **2015**, 6, 8817.
[33] H. Tian, J. Qin, D. Hou, Q. Li, C. Li, Z.-S. Wu, Y. Mai, *Angew. Chem., Int. Ed.* **2019**, 58, 10173.
[34] Y. Fang, Y. Lv, F. Gong, A. A. Elzatahry, G. Zheng, D. Zhao, *Adv. Mater.* **2016**, 28, 9385.
[35] L. Wang, X. Bi, S. Yang, *Adv. Mater.* **2016**, 28, 7672.

- [36] M. S. Zhu, Y. Huang, Q. H. Deng, J. Zhou, Z. X. Pei, Q. Xue, Y. Huang, Z. F. Wang, H. F. Li, Q. Huang, C. Y. Zhi, *Adv. Energy Mater.* **2016**, *6*, 1600969.
- [37] Y. Zhou, Q. Bao, L. A. L. Tang, Y. Zhong, K. P. Loh, *Chem. Mater.* **2009**, *21*, 2950.
- [38] C. Bosch-Navarro, E. Coronado, C. Marti-Gastaldo, J. F. Sanchez-Royo, M. G. Gomez, *Nanoscale* **2012**, *4*, 3977.
- [39] B. Xie, Y. Chen, M. Yu, T. Sun, L. Lu, T. Xie, Y. Zhang, Y. Wu, *Carbon* **2016**, *99*, 35.
- [40] D. Kim, B. Yoo, *Sens. Actuators, B* **2011**, *160*, 1168.
- [41] D. C. Tiwari, P. Atri, R. Sharma, *Synth. Met.* **2015**, *203*, 228.
- [42] I. Rawal, A. Kaur, *Sens. Actuators, A* **2013**, *203*, 92.
- [43] T. N. Ly, S. Park, *Sci. Rep.* **2018**, *8*, 18030.
- [44] X. Tang, J.-P. Raskin, N. Kryvutsa, S. Hermans, O. Slobodian, A. N. Nazarov, M. Debliquy, *Sens. Actuators, B* **2020**, *305*, 127423.
- [45] X. Tang, D. Lahem, J.-P. Raskin, P. Gerard, X. Geng, N. Andre, M. Debliquy, *IEEE Sens. J.* **2018**, *18*, 9088.
- [46] J. Zhao, Y. Liu, X. Li, G. Lu, L. You, X. Liang, F. Liu, T. Zhang, Y. Du, *Sens. Actuators, B* **2013**, *181*, 802.
- [47] M. Q. Yang, N. Zhang, M. Pagliaro, Y. J. Xu, *Chem. Soc. Rev.* **2014**, *43*, 8240.
- [48] J. Ma, Y. Ren, X. Zhou, L. Liu, Y. Zhu, X. Cheng, P. Xu, X. Li, Y. Deng, D. Zhao, *Adv. Funct. Mater.* **2018**, *28*, 1705268.
- [49] J. Zhang, X. Liu, S. Wu, H. Xu, B. Cao, *Sens. Actuators, B* **2013**, *186*, 695.
- [50] H. Xiao, Z.-S. Wu, L. Chen, F. Zhou, S. Zheng, W. Ren, H.-M. Cheng, X. Bao, *ACS Nano* **2017**, *11*, 7284.
- [51] S. Wang, Z.-S. Wu, F. Zhou, X. Shi, S. Zheng, J. Qin, H. Xiao, C. Sun, X. Bao, *npj 2D Mater. Appl.* **2018**, *2*, 7.
- [52] S. Zheng, J. Ma, Z.-S. Wu, F. Zhou, Y.-B. He, F. Kang, H.-M. Cheng, X. Bao, *Energy Environ. Sci.* **2018**, *11*, 2001.
- [53] S. Zheng, Z.-S. Wu, F. Zhou, X. Wang, J. Ma, C. Liu, Y.-B. He, X. Bao, *Nano Energy* **2018**, *51*, 613.
- [54] J. Qin, S. Wang, F. Zhou, P. Das, S. Zheng, C. Sun, X. Bao, Z.-S. Wu, *Energy Storage Mater.* **2019**, *18*, 397.
- [55] S. Zheng, C. Zhang, F. Zhou, Y. Dong, X. Shi, V. Nicolosi, Z.-S. Wu, X. Bao, *J. Mater. Chem. A* **2019**, *7*, 9478.
- [56] F. Zhou, H. Huang, C. Xiao, S. Zheng, X. Shi, J. Qin, Q. Fu, X. Bao, X. Feng, K. Müllen, Z.-S. Wu, *J. Am. Chem. Soc.* **2018**, *140*, 8198.
- [57] W. Gao, N. Singh, L. Song, Z. Liu, A. L. Reddy, L. Ci, R. Vajtai, Q. Zhang, B. Wei, P. M. Ajayan, *Nat. Nanotechnol.* **2011**, *6*, 496.
- [58] Z.-S. Wu, K. Parvez, X. L. Feng, K. Müllen, *Nat. Commun.* **2013**, *4*, 2487.
- [59] B. Song, L. Li, Z. Lin, Z.-K. Wu, K. Moon, C.-P. Wong, *Nano Energy* **2015**, *16*, 470.
- [60] X. Wang, S. Zheng, F. Zhou, J. Qin, X. Shi, S. Wang, C. Sun, X. Bao, Z.-S. Wu, *Natl. Sci. Rev.* **2019**, *6*, 1.
- [61] S. Wang, Z.-S. Wu, S. Zheng, F. Zhou, C. Sun, H.-M. Cheng, X. Bao, *ACS Nano* **2017**, *11*, 4283.
- [62] C. Meng, J. Maeng, S. W. M. John, P. P. Irazoqui, *Adv. Energy Mater.* **2014**, *4*, 1301269.
- [63] K. S. Kumar, N. Choudhary, Y. Jung, J. Thomas, *ACS Energy Lett.* **2018**, *3*, 482.
- [64] P. Zhang, F. Wang, M. Yu, X. Zhuang, X. Feng, *Chem. Soc. Rev.* **2018**, *47*, 7426.
- [65] J. Qin, P. Das, S. Zheng, Z.-S. Wu, *APL Mater.* **2019**, *7*, 090902.